Didier Lasseux[1]
e-mail: didier.lasseux@ensam.eu

Pascal Jolly

TREFLE,
CNRS UMR8508,
University of Bordeaux,
Esplanade des Arts et Métiers,
33405 Talence Cedex, France

Yves Jannot
LEMTA,
CNRS UMR7563 2,
Avenue de la Forêt de Haye-BP 160,
54504 Vandoeuvre Cedex, France

Emmanuel Sauger Benoit Omnes
CETIM-74,
Route de la Jonelière-BP 82617,
44326 Nantes Cedex 3, France

Permeability Measurement of Graphite Compression Packings

In this work, we address the issue of the sealing performance of ring-shape valve compression packings. Our analysis is focused on the characterization of the permeability of the rings made of die-formed exfoliated graphite. Because of the tight character of the material, significant Klinkenberg effects are expected. In addition, due to the manufacturing process, permeabilities k_z and k_r as well as Klinkenberg coefficients b_z and b_r in the respective axial and radial directions are markedly different and strongly dependent upon the applied stress. A specific experimental device based on pressure pulse decay of nitrogen through the material was designed for the measurement in each direction under a controlled axial compression. Determination of k_z and k_r and b_z and b_r is performed on the basis of a nonstationary gas flow model in the radial and axial directions using an inverse procedure applied to the pressure decay signal. Our results confirm the efficiency of the method developed here. They clearly show the anisotropic character of the material (k_z is roughly one order of magnitude larger than k_r) and the dependence upon axial compression. The present analysis is the key step before further quantification of the leak rate that may result from the permeation through the material as envisaged here as well as through interfaces between the housing, the packings, and the stem.
[DOI: 10.1115/1.4002922]

1 Introduction

While chemical leakage through devices such as valves present on piping is estimated to contribute up to 60% of fugitive emission from petrochemical units, sealing efficiency of stem packings is crucial. To improve sealing performance, a thorough characterization of the possible leak paths is required. In fact, while leak may result from both permeation through the porous material of the packings and flow through the stem-packings-housing interfaces, the net contribution of each of the two to the total flow rate is not clear so far. However, a relying direct and separate characterization of the two contributions represents a very difficult problem. An alternative two-stage strategy underlying the present work is first to characterize the packing material itself, i.e., the permeation through the porous material, and second to determine the total leak in a real configuration so that the contribution of the interfacial flow can be inferred. The aim of this work is hence to contribute to the diagnosis of packing tightness efficiency by addressing the first of these two stages through permeability measurement of the packing material only. Our analysis is focused on die-formed exfoliated graphite compression packings. Since these materials are selected for their low permeability, the measurement of this quantity is a tricky task that requires specific techniques. Packings under investigation are rings whose permeability k_z and k_r in the axial and radial directions, respectively, are expected to be significantly different as a consequence of their manufacturing process. Moreover, k_z and k_r are expected to depend on the stress applied to the material. A special measurement device for each direction of investigation is hence necessary for their determination. Both devices are designed for a controlled axial compression to be applied.

Because these materials are expected to have very small permeabilities, the use of a steady-state gas flow method, although appealing, is not well adapted. In fact, this can lead to excessively long experiments since the characteristic time to reach steady-state flow typically varies with the inverse of the permeability and the square of the sample length in a 1D experiment. Moreover, in this permeability range, important Klinkenberg effects are expected [1] unless the mean gas pressure within the sample is relatively high. If performed on the basis of a steady-state method, the measurement hence requires several different experiments carried out at different mean pressure levels [2,3]. In addition, precise measurement of gas flow rates in this type of experiment remains a difficult task. Conversely, an unsteady-state gas flow is much faster and, as detailed below, allows simultaneous determination of k and b. The use of this method was initiated in the early 1950s [4] and has been the subject of many studies until recently [5–11]. The unsteady-state experiment basically consists in recording the pressure difference between two gas chambers connected to the sample edges, the upstream one being suddenly submitted to a pressure larger than the equilibrium one featuring what is often referred to as a pulse-decay experiment.

Recently, we have clearly shown that the optimal configuration from the point of view of the pressure signal sensitivity to the parameters k and b is the so-called draw-down experiment, a variant of the pulse-decay. In this configuration, the downstream chamber has an infinite volume, which means that the downstream face of the sample remains at the atmospheric pressure [12]. With this method, the sample to be tested does not need to be preconditioned at a high gas-pressure level. This last option was however often considered in the literature to eliminate Klinkenberg effects but has the main drawback of requiring an equilibrium stage at this pressure level, which can be very lengthy as indicated above.

In many reported analysis on this unsteady-state technique, interpretation of the pressure decay signal is often carried out by assuming that the gas flow is insensitive to accumulation effects in the pores (i.e., that the mass flow rate does not explicitly depends on time) and/or that Klinkenberg effects are negligible. In this work, we do not retain this hypothesis and a more complete method to interpret our experiments is developed in addition to the two specific experimental draw-down setups that were designed for the measurement of transport coefficients in the radial and axial directions. The analysis allows estimating k_z and k_r and Klinkenberg coefficients, b_z and b_r (as well as the porosity ε), of the material at the axial compression level under investigation.

[1]Corresponding author.

Contributed by the Pressure Vessel and Piping Division of ASME for publication in the JOURNAL OF PRESSURE VESSEL TECHNOLOGY. Manuscript received September 10, 2009; final manuscript received October 18, 2010; published online May 16, 2011. Assoc. Editor: Hakim A. Bouzid.

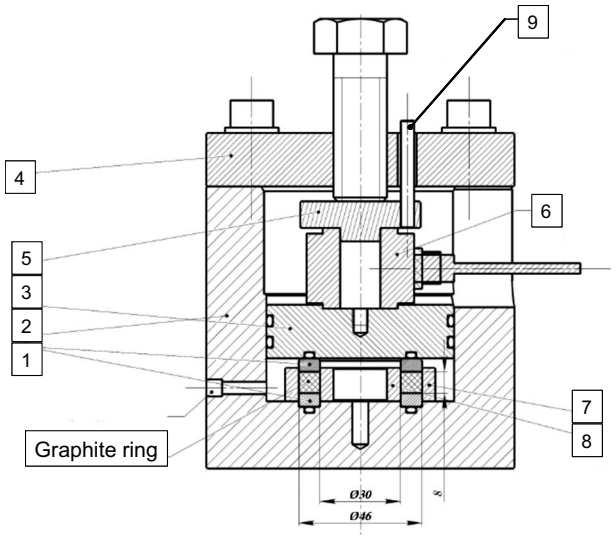

Fig. 1 Experimental device designed for the measurement of the radial permeability

Estimation is performed on the basis of a creeping, nonstationary, isothermal, and weakly compressible gas flow model along with an inverse technique. Our results indicate that the procedure and the technique employed here to estimate k_z and k_r and b_z and b_r are efficient. Estimated permeabilities are in the range 10^{-20}–10^{-21} m^2, while k_z is roughly one order of magnitude larger than k_r. Permeabilities in both directions (as well as b_z and b_r) are significantly affected by the axial compression. The perspective of this work is to compare the leak rate that can be estimated from the present analysis to that observed on a valve. In this last configuration, leak may result from the permeation through the packing material, on the one hand, and from the flow through interfaces between the housing, the packings, and the stem, on the other.

2 Experimental Technique

In this section, the two specific experimental devices developed for the measurement of the permeability and Klinkenberg coefficient in the radial and axial directions are presented. Graphite rings employed in the tests have an inner radius $r_0=15$ mm, an outer radius $r_1=23$ mm, and a height $h=8$ mm.

2.1 Experimental Device for the Measurement of k_r and b_r. The experimental device to measure the permeability k_r and Klinkenberg coefficient b_r (and porosity ε) of the die-formed exfoliated graphite rings in the radial direction is schematically represented in Fig. 1. It basically consists of a rigid frame (item 2) closed by a flange (item 4). Within this assembly, high- and low-pressure gas chambers are formed, corresponding respectively to the inner and outer regions of the ring. To measure k_r and b_r, the graphite ring must be sealed axially to avoid flow in this direction. To do so, two metal rings (item 1) are glued on the upper and lower faces of the ring. Sealing between the upper and lower axial faces of this three-ring assembly (graphite and metal rings) is achieved using O-rings placed between the lower metal ring and the frame on the one hand and the upper metal ring and the piston (item 3) on the other. Two other O-rings placed in grooves of the piston ensure tightness between the low-pressure (or downstream) chamber and the outside of the device. The high-pressure (or upstream) chamber and the downstream one can be connected to external tanks if required; i.e., the experiment can be run in the pulse-decay configuration.

Tests are performed in a configuration identical to that in the real situation. In particular, graphite rings undergo a controlled axial compression. The compression stress, σ, is applied to the graphite ring by means of a screw-nut system. It is transmitted from the screw to the graphite ring through the piston, the load cell (item 6), allowing the measurement and the control of the axial compressive force, and a centering ring (item 5). A displacement sensor (not represented in Fig. 1), whose finger is placed on a pin (item 9), is used to measure the axial corresponding deformation.

In addition, as in the real situation, internal and external radial displacements are limited by rigid and highly permeable rings (items 7 and 8). These two rings play the role of the stuffing box and stem and are made of sintered bronze. Their intrinsic permeability is roughly 3×10^{-14} m^2, a value which is far larger than those expected for the graphite rings (see results below). As a consequence, their pressure drop contribution to the flow, both from the viscous and Klinkenberg effect points of view, can be safely neglected in the interpretation of the pressure signal to estimate the intrinsic properties of the graphite rings.

To validate the design of the device and control the sealing efficiency of the assembly, sealing tests were carried out. For these tests, the graphite ring was replaced by an impermeable metal ring, and the change in the initial pressure of typically 50 bars was recorded in the upstream chamber closed for a period of several days without noticing any decrease.

As detailed below, permeability and Klinkenberg coefficient estimation is extracted from the interpretation of an unsteady gas flow through the graphite ring. When the upstream chamber containing the pressurized gas (nitrogen) is opened at the inner part of the ring at $t=0$, gas flows through the material in the radial direction and pressure decreases in the upstream chamber. As justified in the introduction, our experiments were carried out in the draw-down configuration that is optimal for unsteady-state experiments. Consequently, the following measurements are performed during the test:

- Compressive force (load cell range 0–50 kN, precision 20 N). This corresponds to an axial stress range from 0 MPa to 52 MPa and a precision of 0.02 MPa.
- Deformation Δh of the graphite ring due to compression (displacement sensor range ±5 mm, precision 0.02 mm)
- Pressure over time $p_0(t)$ in the upstream chamber until $t=t_f$ (pressure gauge range 0–60 bars, precision 5×10^{-3} bars). In the draw-down experiment used here, the pressure in the downstream chamber remains constant equal to $P_1=P_{atm}$.

For parameters estimation, the volume V_0 of the upstream chamber must be determined. This was performed by replacing the graphite ring by an impermeable metal ring having the same dimensions and by relaxing the pressure of a mass of gas initially confined in a tank of known volume into V_0. The upstream volume was found to be $V_0=38.2\times10^{-6}$ m^3. This volume corresponds to the height of the stress-free graphite ring and is corrected according to the deformation after compression.

The experimental procedure is as follows: Graphite rings are prepared with glued metal rings respecting coaxiality of the assembly which height is measured prior to the test. This assembly is positioned within the experimental device, and the axial compressive force is applied. Two different compression stresses were investigated ($\sigma\sim15.2$ MPa and $\sigma\sim29.3$ MPa). The deformation is measured, and V_0 is recalculated. The last step is the gas pressure relaxation record through the ring from its initial value $P_0=p_0(t=0)$. Typically, P_0 was chosen in the range 5–40 bars. Tests were carried out on different rings, and some of them were repeated several times on the same sample.

2.2 Experimental Device for the Measurement of k_z and b_z. The experimental device to measure the axial permeability k_z of the die-formed exfoliated graphite rings is represented in Fig. 2. As in the radial configuration, the device reproduces the stuffing

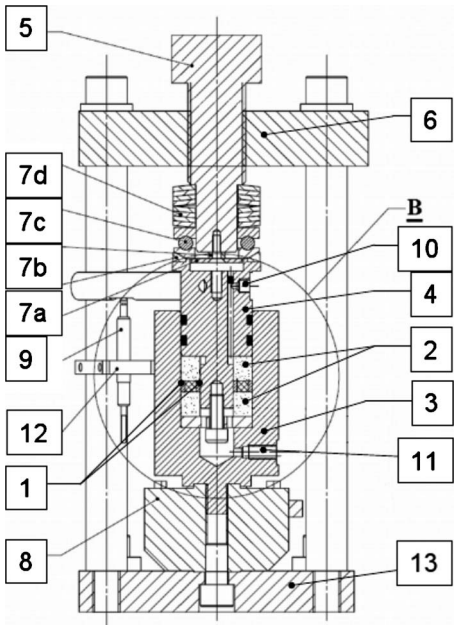

Fig. 2 Experimental device designed for the measurement of the axial permeability

box of a valve. In order to avoid the presence of interfacial leakage and flow in the radial direction, the graphite ring is fitted with two sealing rings (item 1 in Fig. 2) on its inner and outer faces. The assembly is positioned between an upper and a lower porous rings made of sintered bronze (item 2) having the same characteristics as those employed in the radial configuration. These porous rings allow gas flow in the axial direction through the graphite ring and transmission of the axial compressive force. Again, their contribution to the flow of gas can be completely disregarded while interpreting the signal.

The ring assembly is placed inside a cylinder (item 3) that simulates the stuffing box, while a piston (item 4) plays the role of the stem and is used to transmit the axial compressive force. The upstream chamber—including the pore space of the sintered bronze upper ring—formed between the cylinder, the upper face of the graphite ring, and the lower face of the piston is made tight by two O-rings positioned in grooves machined in the piston. Gas is pressurized in this chamber through a connecting orifice (item 10). The downstream chamber is formed between the bottom of the stuffing box and the lower face of the graphite ring and is connected to the atmosphere through the orifice (item 11). Tightness with respect to the upstream chamber is ensured by the two sealing rings (item 1). The compressive force is transmitted to the graphite ring via the piston and the upper porous ring by means of a screw (item 5) moving through the upper flange (item 6). A system made of spring washers, a thrust ball, and a spacer (items 7) was introduced to ensure the axial alignment of the force. Compression is measured with the load cell (item 8) positioned between the cylinder (stuffing box) and the lower flange.

As in the radial configuration, sealing tests were performed, setting an initial pressure of typically 50 bars in the upstream chamber and replacing the graphite ring by an impermeable metal one while checking the pressure change over a period of several days. These conclusive tests allow the validation of the conception of the device from the sealing point of view.

Thus, the experiment consists of the following measurements:

- Compressive force (load cell range 0–50 kN, precision 20 N). The corresponding axial stress range is 0–52 MPa with a precision of 0.02 MPa.
- Deformation Δh of the graphite ring due to compression: This is performed using the displacement sensor (range ± 5 mm, item 9). Precision of this sensor is given by the maximum between 2.5 μm and 0.5% of the measured displacement value.
- Pressure over time $p_0(t)$ in the upstream chamber (pressure gauge range 0–60 bars, precision 5×10^{-3} bars). As in the radial configuration, the downstream chamber is connected to the atmosphere ($P_1=P_{\text{atm}}$) in the context of a draw-down experiment. The change is recorded until $t=t_f$.

Estimation of the permeability, k_z (and Klinkenberg coefficient b_z, as well as porosity ε, see below) is made by interpreting the upstream pressure signal decay using a physical model that is developed in the following sections and requiring the knowledge of V_0, the volume of the upstream chamber. Using the same technique as in the radial case, we found $V_0=35.71\times10^{-6}$ m^3, a value that is not subjected to variations after compression provided all parts transmitting the stress are assumed to be infinitely rigid.

The first stage of the experiment is to glue the sealing system onto the graphite ring. Deformation of the graphite ring is then measured after the compressive force is applied. Next is the recording of the upstream pressure variation $p_0(t)$ due to axial gas flow (nitrogen) through the ring. Two axial compression stresses ($\sigma\sim14.3$ MPa and $\sigma\sim28.3$ MPa) were considered in this analysis. The initial upstream pressure, $P_0=p_0(t=0)$, was roughly 45 bars in all our tests. Experiments were repeated on several different rings and, for some of them, several times on the same ring.

All the experiments were performed at room temperature with a fluctuation from 2 °C to 3 °C.

3 Physical Models

In this section, the physical models used to interpret pressure decay signals in the radial and axial configurations are detailed. These models are presented considering the general case of pulse-decay when the upstream and downstream volumes are of finite extent, keeping in mind that the draw-down case is only a particular situation where the downstream volume tends to infinity. The porous sample is assumed to be homogeneous under the form of a ring of inner radius r_0, outer radius r_1, and thickness h. Its porosity is denoted by ε. We assume an isothermal gas flow at very low Reynolds number (this is usually the case in practice) so that no significant inertial (or Forchheimer) effects are present. In addition, gas is considered as ideal, which is a valid approximation for gases such as N_2 at experimental operating pressures used here. Under these circumstances, the general form of the mass and momentum conservation equations can be written as

$$\varepsilon\frac{\partial\rho}{\partial t}+\nabla\cdot(\rho\mathbf{v})=0 \tag{1}$$

Here, ρ is the gas density and $\mathbf{v}$ the filtration velocity through the porous medium given by Darcy's law including Klinkenberg effects:

$$\mathbf{v}=\frac{\mathbf{K}}{\mu}\cdot\left(\mathbf{I}+\frac{\mathbf{B}}{p}\right)\cdot\nabla p \tag{2}$$

In this last relationship, $\mathbf{K}$, $\mathbf{B}$, and $\mathbf{I}$ are the intrinsic permeability, Klinkenberg correction, and unit tensors, respectively. The ideal gas law is given by

$$\rho=\frac{p}{R_G T} \tag{3}$$

where p and T are the pressure and temperature, respectively, of the gas at a given time and position in the porous medium and R_G is the constant for the gas under consideration ($R_G=R/M$ with $R=8.314$ J mol^{-1} K^{-1}, M being the molar mass of the gas, $R_G=296.93$ J kg^{-1} K^{-1} for nitrogen). These equations are now used

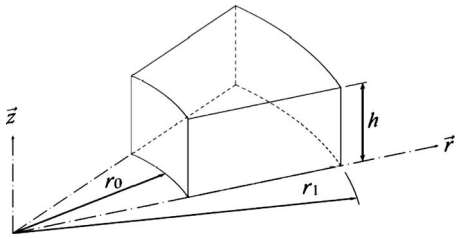

Fig. 3 Annular section of the porous ring

to derive the complete initial boundary value problem in each direction in order to interpret our experiments.

3.1 Radial Direction. We first consider a pressure gradient in the radial direction (see Fig. 3), i.e., $\nabla p=(\partial p/\partial r)\mathbf{e_r}$. As in the sequel of this paper, we assume that the principal axes of **K** and **B** are $\mathbf{e_r}$ and $\mathbf{e_z}$, respectively. Along with the fact that the material is homogeneous, this leads to a pure radial flow so that $p=p(r,t)$. Under these circumstances, the combination of Eqs. (1)–(3) leads to the following time and space distribution of pressure:

$$\frac{\mu\varepsilon}{k_r}\frac{\partial p}{\partial t}=\frac{1}{r}\frac{\partial}{\partial r}\left[r\frac{\partial p}{\partial r}(p+b_r)\right] \tag{4}$$

to which, for completeness, one must associate boundary and initial conditions as specified below.

3.1.1 Boundary Conditions. The upstream boundary condition can be simply derived by writing that the mass flow rate through the upstream or inlet face of the porous sample is exactly that out of the upstream chamber. The mass flow rate through the inlet face of section S_0 at $r=r_0$ can be written as

$$q_m=\rho_0 v_0 S_0 \tag{5}$$

where v_0 denotes the filtration velocity in the radial direction at the inlet face of the ring as given by Eq. (2). If p_0 denotes the pressure on this face of the ring ($p_0=p(r=r_0,t)$), which is equal to that in the upstream chamber, and when ideal gas and Darcy's laws are taken into account, this flow rate can be expressed as

$$q_m=-2\pi r_0 h\frac{p_0}{R_G T}\frac{k_r}{\mu}\left(1+\frac{b_r}{p_0}\right)\left.\frac{\partial p}{\partial r}\right|_{r=r_0} \tag{6}$$

If the experiment is performed at constant temperature, the mass flow rate out of the chamber is simply

$$q_m=\frac{dm}{dt}=-\frac{V_0}{R_G T}\frac{\partial p_0}{\partial t} \tag{7}$$

m being the mass of gas at t in this chamber. Matching the two above expressions leads to the boundary condition at the upstream face given by

$$\frac{\partial p_0}{\partial t}=\frac{2\pi k_r r_0 h}{\mu V_0}(p_0+b_r)\left.\frac{\partial p}{\partial r}\right|_{r=r_0}\quad \text{at } r=r_0 \tag{8}$$

Following the same lines, the boundary condition at the outer (downstream) face of the sample can be readily written as

$$\frac{\partial p_1}{\partial t}=-\frac{2\pi k_r r_1 h}{\mu V_1}(p_1+b_r)\left.\frac{\partial p}{\partial r}\right|_{r=r_1}\quad \text{at } r=r_1 \tag{9}$$

where $p_1=p(r=r_1,t)$. Note that in the case of the draw-down ($V_1\to\infty$), this last condition is simply replaced by a classical Dirichlet condition on the pressure,

$$p_1(t)=Cst=P_1\quad \text{at } r=r_1 \tag{10}$$

3.1.2 Initial Condition. At the initial stage of the experiment, the system is at equilibrium at a pressure equal to the downstream pressure leading to

$$p(r,t)=P_1,\quad t=0,\quad r_0<r\le r_1 \tag{11}$$

Gas flow through the material starts at $t=0$ when the upstream chamber at pressure $P_0>P_1$ is connected to the inner face of the ring, yielding the following condition:

$$p_0=P_0,\quad t=0,\quad r=r_0 \tag{12}$$

As will be detailed below, this initial boundary value problem has no simple analytical solution and requires a numerical treatment.

3.2 Axial Direction. In this section, we consider that the pressure gradient is along $\mathbf{e}_z$ only, leading to a flow along this axis, i.e., $p=p(z,t)$. Combining the mass and momentum equations and the ideal gas law yields the following pressure equation [12]:

$$\frac{\mu\varepsilon}{k_z}\frac{\partial p}{\partial t}=\frac{\partial}{\partial z}\left[\frac{\partial p}{\partial z}(p+b_z)\right] \tag{13}$$

3.2.1 Boundary Conditions. Boundary conditions at the upstream and downstream faces are obtained using the same arguments as in the radial configuration. The upstream face of the sample is taken at $z=0$ and the downstream one is taken at $z=h$, thus leading to

$$\frac{\partial p_0}{\partial t}=\frac{\pi k_z(r_1^2-r_0^2)}{\mu V_0}(p_0+b_z)\left.\frac{\partial p}{\partial z}\right|_{z=0}\quad \text{at } z=0 \tag{14}$$

and

$$\frac{\partial p_1}{\partial t}=-\frac{\pi k_z(r_1^2-r_0^2)}{\mu V_1}(p_0+b_z)\left.\frac{\partial p}{\partial z}\right|_{z=h}\quad \text{at } z=h \tag{15}$$

In these equations, p_0 and p_1 are, respectively, $p(z=0,t)$ and $p(z=h,t)$. The latter condition reduces to

$$p_1(t)=Cst=P_1\quad \text{at } z=h \tag{16}$$

in the draw-down condition.

3.2.2 Initial Conditions. Just as in the radial direction, the initial condition is simply given by

$$p(z,t)=P_1,\quad t=0,\quad 0<z\le h \tag{17}$$

the flow being initiated at $t=0$ by the pressure P_0 at the upstream face, i.e.,

$$p_0=P_0,\quad t=0,\quad z=0 \tag{18}$$

For subsequent interpretation of experimental data, this problem is solved numerically.

For each configuration (radial and axial), the initial and boundary value problems presented above is discretized using a finite difference scheme that is second order in space and explicit first order in time. A stability condition of the scheme must be ensured by a time step condition given by $\Delta t<\alpha_x(\Delta x)^2/2[p_0(t=0)+b_x]$, with $\alpha_x=\mu\varepsilon/k_x$, $x=r$ or z, depending on the radial or axial configuration. The numerical solution resulting from the direct simulation yields $p_0(t)$, which quadratic deviation with respect to the measured signal is minimized using an inverse algorithm to estimate the desired parameters.

4 Inversion and Results

Our inverse technique is a Levenberg–Marquardt algorithm developed to simultaneously estimate k_x and b_x, $x=r$ or z (as well as ε, see below). This method combines a Gauss–Newton method with a gradient descent, one taking benefits of the rapidity of the former and of the stability of the latter. Details of the algorithm can be found, for instance, in Refs. [13,14]. Basically, it consists in minimizing the square of the χ function given by $\chi^2(k_x,b_x)=\Sigma_{i=1}^{N}\{[p_{0m}(t_i)-p_0(t_i)]/\sigma_i\}^2$, $x=r$ or z. In this formula, N is the

number of time records of the measured signal p_{0m}, p_0 is the value of the upstream pressure estimated from the model at a given set of parameters (k_x, b_x, and ε), and σ_i is the standard deviation on p_{0m} at the ith time record. Convergence is achieved once χ^2 falls below a user-defined criterion chosen here equal to 0.05.

To start the inversion process, it is necessary to provide initial values of k_x, b_x, $x=r$ or z, and ε. These values were extracted from a simplified interpretation of the flow based on a hypothesis often proposed in the literature [7]. It consists in assuming that gas density is not explicitly time dependent, meaning that gas accumulation in the pore space is negligible. This hypothesis is asymptotically valid when $p_0(t)$ reaches P_1. For this reason, we used the late part of the recorded values of $p_0(t)$, i.e., the last 10% of the experimental signal. In the case of the draw-down experiment, this allows to pre-estimate k_r and k_z, according to the following expressions:

$$k_r = -\frac{V_0 \mu \ln\frac{r_1}{r_0}}{2\pi h[p_0(t)-P_1]\left(b_r + \frac{p_0(t)+P_1}{2}\right)}\frac{dp_0}{dt} \tag{19}$$

in the radial case and

$$k_z = -\frac{V_0 \mu h}{\pi(r_1^2 - r_0^2)[p_0(t)-P_1]\left(b_z + \frac{p_0(t)+P_1}{2}\right)}\frac{dp_0}{dt} \tag{20}$$

in the axial case. These two relationships can be completed with pre-estimated values of b_r and b_z using an empirical correlation proposed in [7]: $b_x = 1,89\times10^{-6}k_x^{-0,36}$, $x=r$ or z where units for k_x and b_x are m^2 and bar, respectively. For ε, an "intermediate" value of around 20% can be used.

Prior to the inversion of experimental signals, we have analyzed the impact of time sampling of $p_0(t)$ as well the influence of errors on experimental parameters such as V_0, r_0, h, and ε on the estimation of k_x and b_x, $x=r$ or z, resulting from inversion. To do so, we have used a synthetic signal $p_0(t)$ generated with a direct numerical simulation. To be more realistic, a random Gaussian noise given by $\delta p = 0,01adpP_0/3$ was superimposed on $p_0(t)$. In this relationship, a is a random number sequence of unit standard deviation and dp is the error on $p_0(t)$ (in percent of the measurement). Coefficient 3 was chosen so that $p_0(t) \pm \delta p$ represents 99.7% of the values of $p_0(t)$ if they would have been measured. Here, we took $dp=0.1\%$. This noisy synthetic signal, generated with the nominal values of the different parameters, was then used as an input of our inversion procedure for which parameters were those embedding an error. The resulting estimation of k_x and b_x, $x=r$ or z, was compared with the initial input values. In accordance with a result already reported in Ref. [15] in the axial case, this analysis leads to the following conclusions for both the radial and axial configurations: (i) Time sampling is not a crucial parameter to correctly estimate k_x and b_x, $x=r$ or z. This is an indication that no significant precision can be gained from increasing the number of points to sample $p_0(t)$ over a given period of time; (ii) an error on V_0, r_0, or h does not yield significant errors on the estimated values of the permeability or Klinkenberg coefficient; (iii) an error on ε has a very important impact on the estimation of these parameters. From a practical point of view, ε and its evolution with the compression stress are not known precisely a priori. For this reason, k_x, b_x, $x=r$ or z, and ε were estimated simultaneously. Without detailing all the features of the inverse technique, it must be noted however that the sensitivity of the pressure signal to the porosity is much less than the sensitivity to the permeability and Klinkenberg coefficient. Interpretation of our experimental data is presented in the next sections.

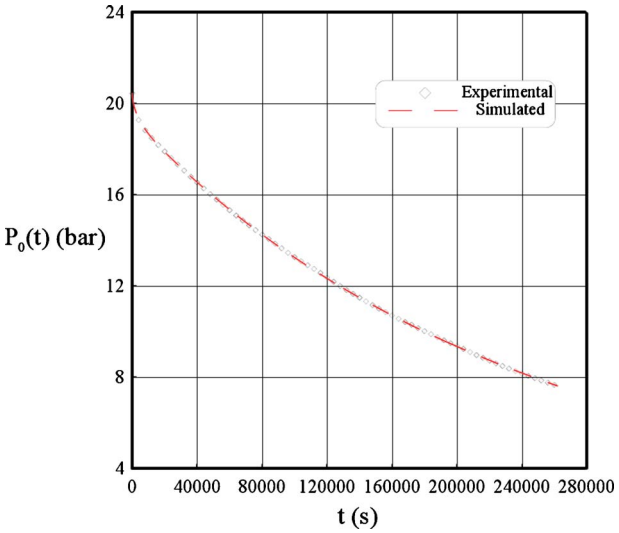

Fig. 4 Experimental pressure signal (open symbols) and $p_0(t)$ simulated with the estimated values of the parameters. Radial case. Ring 6, test 2. Compression stress 14.2 MPa and P_0 =20.4 bars.

4.1 Results in the Radial Configuration. Experiments in this configuration were performed on six different rings for σ in the range 14.2–17.0 MPa and in the range 29.1–29.9 MPa on the five first ones only.

To illustrate the inversion procedure, we have reported in Fig. 4 an example of a recorded experimental pressure signal (open symbols) along with the simulated evolution of p_0 obtained with estimated values of the parameters k_r, b_r, and ε resulting from inversion.

Although the comparison in this figure is not sufficient to check the validity of the inversion, our physical model seems to correctly reproduce the evolution of the pressure observed at the upstream face of the ring. A better quantitative verification of the estimation of the parameters is made by analyzing the residuals after inversion, i.e., the difference between the measured signal and the simulated one. This is represented in Fig. 5, showing that these residuals remain less than 80 mbars that is on the order of 1% of the smaller pressure measured during the experiment (i.e., at $t=t_f$).

A quick comparison between these residuals and the evolution

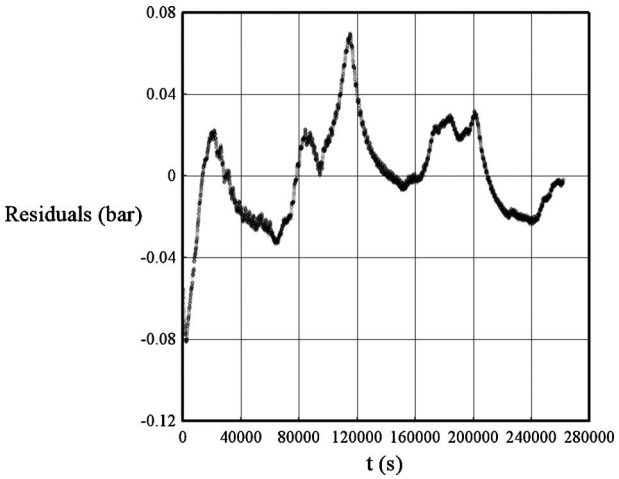

Fig. 5 Residuals between the measured and estimated pressure signals. Radial case. Ring 6, test 2. Compression stress 14.2 MPa and P_0=20.4 bars.

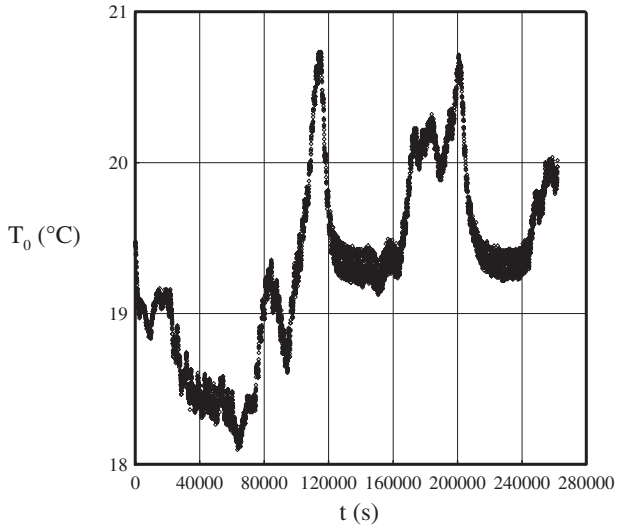

Fig. 6 Gas temperature in the upstream reservoir. Radial case. Ring 6, test 2. Compression stress 14.2 MPa and P_0 =20.4 bars.

of the gas temperature in the upstream chamber as represented in Fig. 6 indicates that the residuals have a strong signature of the temperature fluctuations. Since this thermal effect is not accounted for in the physical model, its effect remains a perturbation source in the inversion process. All the results obtained in the lower range of stress are gathered in Table 1.

Except on ring 4, the deformation is roughly from 0.9 mm to 1 mm, which represents 11% to 12% of the ring thickness when it is free of stress. Estimated values of the radial permeability, Klinkenberg coefficient and porosity (see Table 1) show that except on ring 6, k_r is in the range 4.9×10^{-21}–6.9×10^{-21} m^2 (average 6.2×10^{-21} m^2), while b_r is in the range 8.4–10 bars (average 9.2 bars), which remains relatively narrow while taking into account the order of magnitude of this permeability as well the variability on the material inherent to the manufacturing process. The variability is evidenced with ring 6, having a smaller permeability in the range 1.5×10^{-21}–3.5×10^{-21} m^2 over the three different tests, whereas b_r, except for the second test, is around 16–19 bars.

Estimated values of the porosity on the six samples are more spread, in the range 21–46% (average 33.6%). A plausible explanation of such a distribution lies again in the variability of the material as a result of the manufacturing process. This spread might also include the error on the estimation of this parameter since the sensitivity of the pressure decay to ε remains small compared with the permeability and Klinkenberg coefficient. This feature is even more pronounced in this low range of permeability.

When the axial compression stress is increased by roughly a factor of 2 (see results gathered in Table 2), the deformation increases ($\Delta h\sim1.4$ mm except again for ring 4) while the permeability decreases by roughly a factor of 2 (average 3.6×10^{-21} m^2) and, accordingly, b_r increases (average 12.3 bars).The porosity remains roughly in the same range (average 33.5%). This would indicate that larger flow-path constrictions were reduced in the radial direction while increasing the axial compression although no significant global compaction of the bulk material occurred.

4.2 Results in the Axial Configuration. Experiments were carried out on three different rings and for the two ranges of axial compression stress (13.6 MPa$\leq\sigma\leq$14.7 MPa and 27.2 MPa $\leq\sigma\leq$29.3 MPa). Again, to check the result of the inversion process, we have represented in Fig. 7 the evolution of p_0 measured on ring 7 for σ=29.3 MPa along with the simulated pressure signal obtained with the estimated values of the parameters in this case.

As in the radial case, the overall approach is validated by the residuals between the measured pressure decay and that predicted by the direct model as represented in Fig. 8. These residuals remain smaller than 150 mbars (and even 80 mbars if the very early stage of the experiment is ignored) and are strongly correlated with the temperature fluctuations in the upstream gas chamber represented in Fig. 9. Results obtained in this configuration are gathered in Table 3.

For the lower stress range, the deformation is again about 1 mm

Table 1 Results on six different rings obtained in a range of compression stress 14.2–17.0 MPa. Radial case.

Ring No.	σ (MPa)	P_0 (bar)	$P_0(t_f)$ (bar)	Δh (mm)	k_r (m^2)	b_r (bar)	ε (%)
1	14.7	9.40	8.58	0.98	6.7×10^{-21}	9.6	28.0
2	14.7	9.36	8.51	0.98	4.9×10^{-21}	9.2	35.0
3	15.7	4.98	3.87	0.92	6.6×10^{-21}	8.4	36.1
4	15.9	7.69	5.51	1.4	6.9×10^{-21}	8.6	45.7
5	16.9	11.12	7.93	0.92	5.7×10^{-21}	9.9	33.9
6_1	14.8	39.77	2.73	0.92	2.7×10^{-21}	18.9	21.2
6_2	14.3	20.42	7.60	0.92	1.5×10^{-21}	47.1	33.1
6_3	14.2	19.61	9.58	0.90	3.5×10^{-21}	16.1	35.5

Table 2 Results on five different rings obtained in a range of compression stress 29.1–29.9 MPa. Radial case.

Ring No.	σ (MPa)	P_0 (bar)	$P_0(t_f)$ (bar)	Δh (mm)	k_r (m^2)	b_r (bar)	ε (%)
1	29.9	10.4	9.8	1.52	3.6×10^{-21}	11.0	20.8
2	29.2	10.4	10.0	1.4	2.4×10^{-21}	13.6	31.6
3	29.3	6.6	5.5	1.32	4.1×10^{-21}	8.2	35.7
4	29.5	7.4	6.0	1.8	4.3×10^{-21}	8.8	43.7
5_1	29.1	11.3	9.0	1.46	4.4×10^{-21}	7.0	37.0
5_2	29.1	23.3	20.6	1.46	2.5×10^{-21}	12.8	32.1

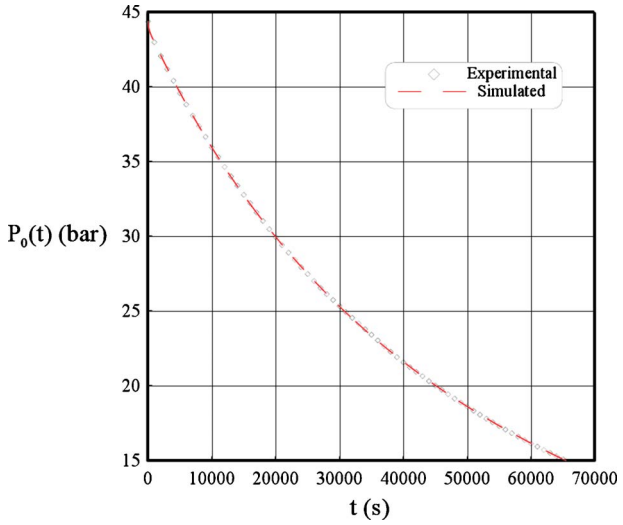

Fig. 7 Experimental pressure signal (open symbols) and $p_0(t)$ simulated with the estimated values of the parameters. Axial case. Ring 7 and compression stress 29.3 MPa and P_0 =44.4 bars.

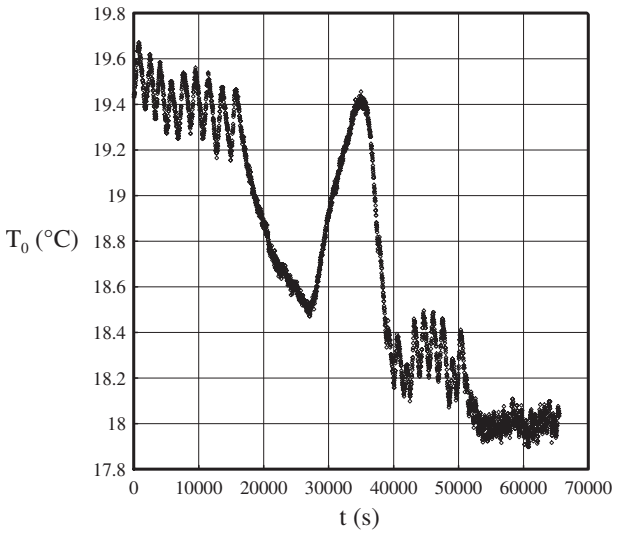

Fig. 9 Gas temperature in the upstream reservoir. Axial case. Ring 7 and compression stress 29.3 MPa and P_0=44.4 bars.

and increases to roughly 1.2 mm when this stress is increased by a factor of 2, confirming the observation already reported in the radial case. Estimated parameters k_z, b_z, and ε on the three different rings remain in a narrow range centered on the average values, respectively, given by 6.4×10^{-20} m^2, 17.3 bars, and 19.7% for 13.6 MPa$\leq\sigma\leq$14.7 MPa and 2.8×10^{-20} m^2, 20.0 bars, and 18.8% for 27.2 MPa$\leq\sigma\leq$29.3 MPa. As expected, k_z decreases (again by a factor close to 2 when the stress is doubled as in the radial case) while b_z increases. It shall be noted that all the values of b_z are very well predicted by the correlation proposed in Ref. [7] mentioned above (see right column of Table 3). Values of the porosity are much less spread than in the radial case. This might result from the fact that the sensitivity to this parameter is larger in this case. In addition, it must be noted that as observed on experiments in the radial direction, porosity very slightly decreases while increasing σ.

More important is the contrast between k_r and k_z for each stress range. In fact, for both ranges of the compression stress, k_r is an order of magnitude smaller than k_z. This clearly highlights the strong anisotropic character of the material and the contrast that was expected, considering the manufacturing process of the rings. Indeed, these rings are obtained by rolling up a sheet of exfoliated graphite around an axis corresponding to the ring axis. As a consequence, the axial permeability is expected to be much larger than the radial one, a behavior that is evidenced and quantified by these experiments.

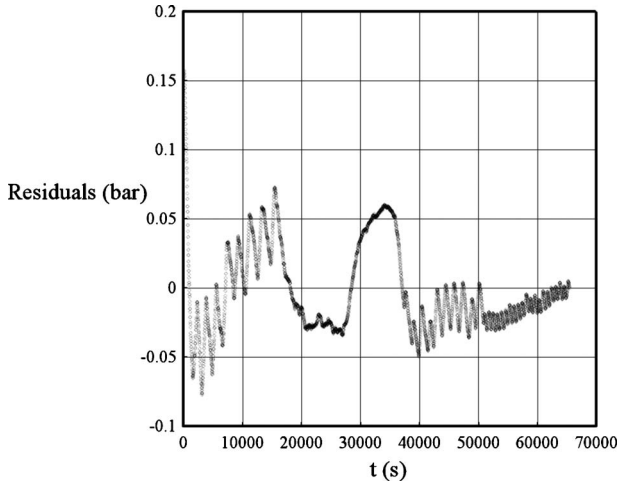

Fig. 8 Residuals between the measured and estimated pressure signals. Axial case. Ring 7 and compression stress 29.3 MPa and P_0=44.4 bars.

5 Conclusions

Based on a previous analysis on the unsteady-state method to measure permeability of tight materials reported in Ref. [12], an experimental procedure and two distinct experimental devices were designed to measure intrinsic permeability (as well as Klinkenberg coefficient and porosity) of die-formed exfoliated graphite compression packings in the radial and axial directions, respectively. The experimental technique consists in recording the pressure decay of a gas confined in a chamber initially pressurized above the equilibrium pressure of the whole system and connected at $t=0$ to the upstream face of the ring, the downstream one remaining at the atmosphere. On the basis of a creeping, nonstationary, isothermal, and weakly compressible flow in a 1D porous medium, an inversion technique was proposed and used on measured pressure decay signals to determine the flow properties of the rings. The whole approach was illustrated on experiments performed on several different rings with two distinct axial compression stresses. Results indicate that (i) the procedure and the technique employed here to estimate permeabilities and Klinkenberg coefficients (as well as porosities) are efficient. Estimated permeabilities are in the range 10^{-20}–10^{-21} m^2; (ii) on this material, axial permeability is roughly one order of magnitude larger than the radial one; (iii) permeabilities in both directions roughly decrease by a factor of 2, while the compression stress is increased from about 14.7 MPa to 29.3 MPa. Klinkenberg coefficients decrease with permeability and are well predicted in the axial direction by an empirical correlation proposed in the literature; (iv) porosities, although more dispersed over all the experiments, seem to very slightly decrease with the axial compression. More work is necessary to improve the estimation of this parameter. Improvements of the experimental procedure can also be achieved with a better thermal regulation of the system.

This work opens wide perspectives for a thorough characterization of the packing materials in order to better qualify and improve the sealing efficiency of industrial valves. In particular, this should allow a further comparison between the leak-rate fraction

Table 3 Results on three different rings obtained in two ranges of compression stress 13.6–14.7 MPa and 27.2–29.3 MPa. Axial case.

Ring No.	σ (MPa)	P_0 (bar)	$p_0(t_f)$ (bar)	Δh (mm)	k_z (m^2)	b_z (bar)	ε (%)	b_{Jones} (bar)
7	13.6	43.94	7.61	1.04	6.1×10^{-20}	17.8	20.1	15.6
8	14.7	44.45	27.68	0.90	5.2×10^{-20}	17.3	19.8	16.6
9	14.7	42.85	5.48	1.06	7.9×10^{-20}	16.9	19.3	14.2
7	29.3	44.37	12.55	1.24	2.2×10^{-20}	21.6	17.1	22.4
8	28.3	44.46	11.14	1.13	2.8×10^{-20}	18.4	21.3	20.6
9	27.2	44.29	7.92	1.33	3.5×10^{-20}	20.1	18.0	19.1

due to permeation through the material of the rings and the total leak-rate of the valve that includes leakage through interfaces between the housing, the packings, and the stem.

Nomenclature

- $\mathbf{B}$ = Klinkenberg correction tensor (Pa)
- b_r = Klinkenberg coefficient in the radial direction (Pa)
- b_z = Klinkenberg coefficient in the axial direction (Pa)
- h = ring thickness (m)
- $\mathbf{K}$ = intrinsic permeability tensor (m^2)
- k_r = permeability in the radial direction (m^2)
- k_z = permeability in the axial direction (m^2)
- p = gas pressure (Pa)
- p_0 = gas pressure at the inlet face of the sample (Pa)
- P_0 = initial gas pressure in the upstream chamber (Pa)
- p_1 = gas pressure at the outlet face of the sample (Pa)
- P_1 = initial gas pressure in the downstream chamber (Pa)
- q_m = gas mass flow rate (kg s^{-1})
- r_0 = inner radius of the ring (m)
- r_1 = outer radius of the ring (m)
- R_G = gas constant (J kg^{-1} K^{-1})
- t = time (s)
- t_f = final time of the experiment (s)
- T = gas temperature (K)
- $\mathbf{v}$ = filtration velocity (m s^{-1})
- V_0 = volume of the upstream chamber (m^3)
- V_1 = volume of the downstream chamber (m^3)
- ε = porosity
- ρ = gas density (kg m^{-3})
- μ = gas dynamic viscosity (Pa s)
- σ = axial gland stress (MPa)

References

[1] Klinkenberg, L., 1941, "The Permeability of Porous Media to Liquids and Gases," *Drilling and Production Practice*, American Petroleum Institute, New York, pp. 200–213.

[2] Rushing, J., Newsham, K., Lasswell, P., Cox, J., and Blasingame, T., 2004, "Klinkenberg-Corrected Permeability Measurements in Tight Gas Sands: Steady-State Versus Unsteady-State Techniques," Paper No. SPE 89867, pp. 1–11.

[3] Blanchard, V., Lasseux, D., Bertin, H., Pichery, T., Chauveteau, G., Tabary, R., and Zaitoun, A., 2007, "Gas/Water Flow in Porous Media in the Presence of Adsorbed Polymer: Experimental Study on Non-Darcy Effects," SPE Reservoir Eval. Eng., **10**(4), pp. 423–431.

[4] Bruce, G., Peaceman, D., and Hachford, H., 1952, "Calculation of Unsteady-State Gas Flow Through Porous Media," Trans. AIME, **221G**, pp. 1–16.

[5] Aronofsky, J., Wallick, C., and Reichertz, P., 1959, "Method of Measuring Characteristics of Porous Materials," U.S. Patent No. 2,867,116.

[6] Brace, W., Walsh, J., and Frangos, W., 1968, "Permeability of Granite Under High Pressure," J. Geophys. Res., **73**(6), pp. 2225–2236.

[7] Jones, S. C., 1972, "A Rapid Accurate Unsteady-State Klinkenberg Permeameter," Paper No. SPE 3535, pp. 383–397.

[8] Hsieh, P., Tracy, J., Neuzil, C., Bredehoeft, J., and Silliman, S., 1981, "A Transient Laboratory Method for Determining the Hydraulic Properties of 'Tight' Rocks—I. Theory," Int. J. Rock Mech. Min. Sci. Geomech. Abstr., **18**, pp. 245–252.

[9] Neuzil, C., Cooley, C., Silliman, S., Bredehoeft, J., and Hsieh, P., 1981, "A Transient Laboratory Method for Determining the Hydraulic Properties of 'Tight' Rocks—II. Application," Int. J. Rock Mech. Min. Sci. Geomech. Abstr., **18**, pp. 253–258.

[10] Chen, T., and Stagg, P., 1984, "Semilog Analysis of the Pulse Decay Technique of Permeability Measurement," SPEJ, **24**(6), pp. 639–642.

[11] Jones, S. C., 1997, "A Technique for Faster Pulse-Decay Permeability Measurements in Tight Rocks," Paper No. SPE 28450, pp. 19–25.

[12] Jannot, Y., Lasseux, D., Vizé, G., and Hamon, G., 2007, "A Detailed Analysis of Permeability and Klinkenberg Coefficient Estimation From Unsteady-State Pulse-Decay or Draw-Down Experiments," Paper No. SCA2007-08.

[13] Marquardt, D., 1963, "An Algorithm for Least-Squares Estimation of Nonlinear Parameters," SIAM J. Appl. Math., **11**, pp. 431–441.

[14] Gill, P., and Murray, W., 1978, "Algorithms for the Solution of the Nonlinear Least-Squares Problem," SIAM (Soc. Ind. Appl. Math.) J. Numer. Anal., **15**, pp. 977–992.

[15] Jannot, Y., Lasseux, D., Delottier, L., and Hamon, G., 2008, "A Simultaneous Determination of Permeability and Klinkenberg Coefficient From an Unsteady-State Pulse-Decay Experiment," Paper No. SCA2008-09.